Analysis of the dynamics of a blue-violet $In_xGa_{1-x}N$ laser with a saturable absorber

V. Z. Tronciu,[1,*] Minoru Yamada,[1] and R. A. Abram[2]
[1]*Faculty of Engineering, Kanazawa University, 2-40-20, Kodatsuno, Kanazawa, 920-8667, Japan*
[2]*Department of Physics, University of Durham, Durham DH1 3LE, United Kingdom*
(Received 29 September 2003; revised manuscript received 29 April 2004; published 17 August 2004)

We report the results of numerical investigations of the dynamical behavior of a blue-violet InGaN laser with a specially incorporated saturable absorber. We have identified the nature of the bifurcation that occurs in the device dynamics and also the conditions that are necessary for self-pulsating and excitable operations. We also demonstrate the influence of the relevant device parameters on the laser dynamics and show how the properties of the saturable absorber and its position in the device have a considerable influence on the laser behavior. Finally theoretical investigations of the excitable behavior and a confirmation of the excitability properties of an InGaN laser are presented and discussed.

DOI: 10.1103/PhysRevE.70.026604 PACS number(s): 42.55.Px, 42.65.Sf

I. INTRODUCTION

In the last decade violet InGaN laser diodes (LD's) have been the subject of considerable attention, with the studies mainly motivated by the prospect of the application of the devices to high-density optical disk storage and optical data processing [1]. In particular, blue-violet laser diodes are required for CD or DVD systems to increase the disk storage capacity up to 25 Gbytes. As a result of recent research, 400 nm (blue-violet) LD performance has been improved and the lifetime has been extended to over 15 000 hours [2]. Blue-violet CW LD's are already commercially available and several reports have recently appeared concerning the CW operation of blue lasers at room temperature [3–7]. In this paper we consider the phenomena of excitability and self pulsation (SP) in blue-violet InGaN lasers.

The use of self-pulsation is attractive for the reduction of feedback noise [8,9] in CD and DVD systems but since the early investigation of Nakamura *et al.* [10], self-pulsating violet and blue-violet LD's have not been studied in any detail. Although less well known than self-pulsation, excitability is a new and rapidly expanding topic in optics, having initially received much more attention in biology [11] and chemistry [12]. However, in recent years there has been growing interest in excitability in the physics and engineering communities, and recognition that the phenomenon might have device applications in optics. Recently, there have been theoretical predictions of excitability in devices, such as optical cavities and different types of lasers [13–17], and in some cases these predictions have been supported by experimental observation. For example, there is particularly convincing experimental evidence of excitability in a laser with a short external cavity [18]. In addition, an experimental investigation of the excitable properties of a solid-state laser with an intracavity saturable absorber is reported by Larotonda *et al.* [19].

In this paper, we report studies of the dynamics of a multiquantum well InGaN laser with a saturable absorber (SA). In particular, we investigate the self-pulsation and excitable operation of the laser, with particular emphasis on the latter. We start in Sec. II with a description of the laser structure and the theoretical model and the associated equations used to calculate the device behavior. The results of numerical calculations of the device dynamics are presented and discussed in Sec. III and the conclusions are given in Sec. IV.

II. LASER STRUCTURE, MODEL, AND EQUATIONS

Figure 1 shows the structure of the InGaN laser with saturable absorber that has been considered; it consists of a multiquantum well (MQW) InGaN active layer and a saturable absorber in the form of a single *p*-type InGaN quantum well. Relatively thin saturable absorber layers varying from 1 to 3 nm have been used with a view to maintaining a low threshold current. The AlGaN layer prevents significant carrier overflow from the active region. In the fabrication process, the saturable absorber layer was grown as a layer parallel to the active region, which is different from the situation treated in previous papers where the SA's were grown perpendicular to the active region [20–23]. Further details on the fabrication method are given by Ohno *et al.* [24]. The lasing wavelength is at 395 nm and three different cavity

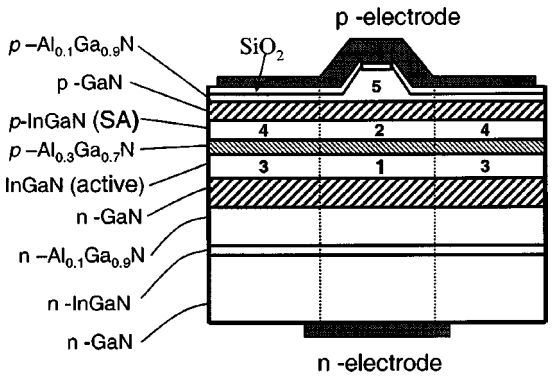

FIG. 1. Schematic illustration of the blue-violet InGaN laser with a saturable absorber incorporated.

*Email address: tronciu@ec.t.kanazawa-u.ac.jp

lengths 350, 500, and 650 μm, have been investigated experimentally.

To model the laser properties we used the Yamada model [20,21] adapted to the specific case of the InGaN laser with saturable absorber incorporated as a layer parallel to active region. The equations of laser operation are

$$\frac{dS}{dt} = \left[\sum_i a_i \xi_i (N_i - N_{gi})/V_i - BS - G_{th} \right] S + M \sum_i a_i \xi_i N_i / V_i, \tag{1}$$

$$\frac{dN_i}{dt} = -\frac{a_i \xi_i}{V_i}(N_i - N_{gi})S_i - \frac{N_i}{\tau_{si}} + \sum_{j \neq i} \left(\frac{N_j}{T_{ji}} - \frac{N_i}{T_{ij}} + \frac{(I_{ji} - I_{ij})}{e} \right), \tag{2}$$

where S is the photon number, N_i is the injected carrier number in the ith region, a_i is the differential gain coefficient, ξ_i is the field confinement ratio, and N_{gi} is the carrier number at transparency. τ_{si} is the carrier lifetime and T_{ij} is an equivalent lifetime giving the carrier diffusion from the j to i region. I_{ij} gives the carrier injection from the j to i region. The second term in the photon rate equation describes the spontaneous emission and M is the equivalent total number of the longitudinal modes, which is evaluated from the half width of the linear gain spectrum. V_i is the volume expressed by $V_i = W_i d_i L$, where L is the laser length and d_i and W_i are the thickness and width, respectively, of the relevant region. The term involving B describes the self-saturation of the gain and implies a nonlinearity of the system. The coefficient B is given by $B = B_C(N_1 - N_{g1})(a_1 \xi_1^2 / V_1^2)$, where

$$B_c = \frac{9\pi c \tau_{\text{in}}^2 |R_{cv}|^2}{2\varepsilon_0 n_r^2 \hbar \lambda_0} \tag{3}$$

and n_r is the refractive index, λ_0 is the central wavelength of the laser, R_{cv} is the dipole moment, and τ_{in} is the intraband relaxation time. The threshold gain level G_{th} is given by

$$G_{\text{th}} = \frac{c}{n_r}\left(k + \frac{1}{2L} \ln \frac{1}{R_f R_B} \right), \tag{4}$$

where R_f and R_b are the reflectivies of the front and the back facets, respectively and κ is the loss coefficient.

The laser structure in Fig. 1 an be considered to be made up of central and outer regions. In the numerical calculations, we take into account four dynamical regions: the central active region 1 and saturable absorber 2 as well as the outer regions 3 and 4. The other regions have been taken into account for the calculation of the effective refractive index, near field patterns and confinement factors. Region 5 is a cap layer, which is electrically connected to the external current source. The field distribution in the transverse cross section is analyzed by the effective refractive index method [25], where the spatial variation of the refractive indices and the gain-loss properties of the media are taken into account. Each region of the device shown in Fig. 1 is taken to have a refractive index which is dependent on its alloy composition and the wavelength of the radiation. The field confinement factors ξ_i of the regions 1–4 are not constant and have been evaluated during the pulsations [20]. The equivalent volumes of the outer regions 3 and 4 also vary and were evaluated with the electron distribution width in these regions [20].

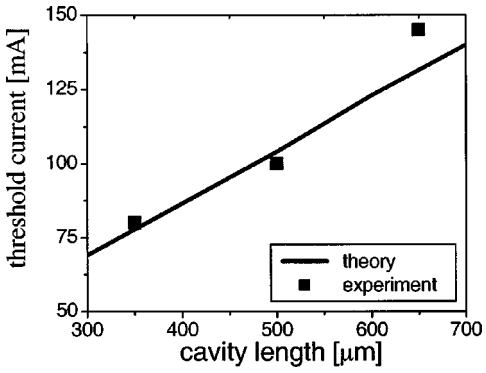

FIG. 2. Dependence of the threshold current on the cavity length. The SA has a thickness of 3 nm and a carrier lifetime of 0.1 ns. The other parameters are given in Table I.

III. RESULTS AND DISCUSSION

Figure 2 shows the theoretical (solid line) and experimental (squares) results obtained for the dependence of the threshold current on cavity length for the laser of Fig. 1. The values of the parameters used in the simulations are listed in Table I. The experiments were carried out at room temperature and the characteristics were measured using a pulsed current, in an effort to avoid heating. Theory predicts that the threshold current should increase from 80 to 125 mA as the cavity length increased from 350 to 650 μm. The theoretical results are broadly supported by experiment; although there is a discrepancy in the predicted and measured threshold currents for the 650 μm cavity, we believe that is due to significant heating of the device that occurred despite the precautions taken. Note that the inclusion of a SA acts to increase the threshold current of the laser. For example, a laser of similar design and a cavity length of 500 μm, but without a SA, recently exhibited a measured threshold current of 29 mA [26], compared to the value of 100 mA found for a device of the same length with a SA.

To understand the properties of the laser, we have considered the laser dynamics in terms of bifurcation diagrams. Figure 3 is an example of such a diagram and shows the calculated peak photon number versus injected current for a laser with a cavity length of 500 μm. As the injected current is increased above threshold CW operation is observed and the corresponding photon number is given by thin solid line near the left side of Fig. 3. At a certain current, denoted by the left hand solid circle in the figure, there is a Hopf bifurcation and the laser begins to pulsate. The thick line to the right of the solid circle gives the peak photon number in the pulsations. As the injected current is increased further the pulsation amplitude goes through a maximum before vanishing at the upper Hopf point denoted by the right hand solid circle. Both Hopf points are supercritical and the characteristic is essentially different from the other self-pulsating lasers reported in Refs. [20,22,23], where SP starts right at the

TABLE I. Parameters used in numerical calculations.

Symbol	Definition	Value and units	
		Active region	SA
a	Differential gain coefficient	1.85×10^{-12} m^3 s^{-1}	13.0×10^{-12} m^3 s^{-1}
N_g	Transparent carrier density	1.4×10^{25} m^{-3}	2.6×10^{25} m^{-3}
τ_s	Carrier life time	2.0 ns	0.1 ns
d	Thickness	18–21 nm	1–3 nm
W	Width	2.0 μm	2.0μm
	Other parameters		
λ	Central wavelength	395 nm	
κ	Loss coefficient	15 cm^{-1}	
I_l	Leak current	0.35I	
R_b	Reflectivity at back facet	0.95	
R_f	Reflectivity at front facet	0.20	
n_r	Refractive index	2.6	
Bc		5.0×10^{-21}	

threshold current. This difference in behavior may be a result of the different carrier lifetimes in the active region and in the SA. In some of our devices, the SA layer has an interface with the AlGaN evaporation prevention layer [24] and this may reduce the carrier lifetime in the SA due to interface-induced nonradiative recombination. Also we found that such a bifurcation diagram with generation of SP through a Hopf bifurcation is appropriate for lasers with a short cavity length.

Now we consider the influence of the carrier lifetime on the laser dynamics for two different values of SA thickness 2 and 3 nm. The carrier lifetime in an InGaN multiquantum well laser diode has been estimated to between 1.8 and 3 ns [1,2] and we have used the value 2 ns in the active region for our calculations. However, for a saturable absorber, recent studies [27] have shown a carrier lifetime in the range 2 ps to 2.5 ns which is dependent on well thickness and bias current. A room-temperature study of the dependence of carrier lifetime on the width of an InGaN single quantum well is reported in Ref. [28], where the carrier recombination was found to be dominated by nonradiative processes. Within the quantum well thickness range from 1 to 6 nm, the carrier lifetime was found to increase from 180 to 340 ps. It has been suggested previously [24] that self-pulsating operation would occur in an InGaN laser with a very short carrier lifetime in the SA. In that work, two lasers were fabricated with the same structure except that one had an additional 20 nm p-type GaN layer between the AlGaN evaporation prevention layer and the SA layer. The results showed that the SP was observed only in the laser without the additional GaN layer, where the carrier lifetime in the SA is small. Figure 4 shows the numerically obtained Hopf bifurcation lines for two different values of the thickness of the SA 2 nm (solid line) and 3 nm (dashed line). It is apparent for a SA of 2 nm thickness that the region of SP can occur for a wide range of carrier lifetime in the active region but for a much narrower range of lifetime in the SA. Also the required carrier lifetime in the SA is much smaller than in the active region. In the case of a 3 nm thick SA, the region of SP is much larger, and also SP can be achieved for a rather higher value of carrier lifetime in the SA but one that is still less than for the active region lifetime. These results reiterate the point that a large carrier lifetime in the active region requires a relatively small lifetime in the SA for SP to occur. However, from these results we can conclude that Hopf lines only appear in the case of lasers with a short cavity length and a low absorption level. We now consider the parameters appropriate to that for excitability detection.

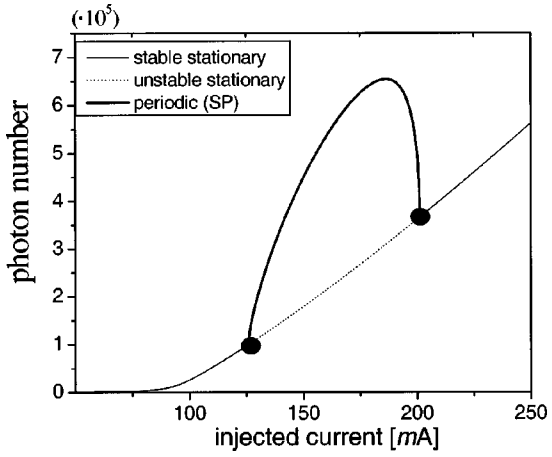

FIG. 3. A bifurcation diagram for a laser with a 500 μm cavity length. The other parameters are as in Fig. 2. The field confinement factors ξ_i of the regions 1–4 for 110 mA injected current are 0.05, 0.02, 0.003, and 0.0003, respectively. The thin solid lines show the stable stationary solutions (CW or nonlasing operation). The thin dotted line shows the unstable stationary solutions (SP operation). The thick solid line shows the periodic solutions. The circles mark the Hopf bifurcation points.

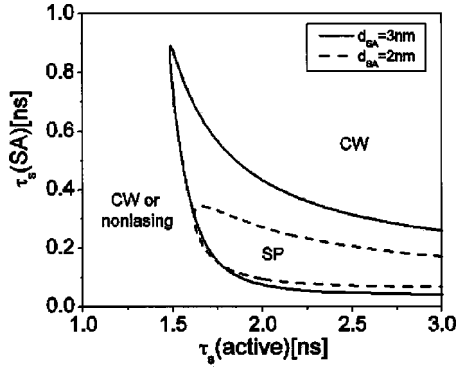

FIG. 4. The bifurcation diagram in the plane of carrier lifetime in the SA vs that in the active region for saturable absorber thicknesses of 2 and 3 nm. The lines denote the Hopf bifurcation points. The cavity length is 500 μm and the injected current is 100 mA. The other parameters are as in Table I.

Excitability in optics is potentially of great interest because of the prospects for applications in optoelectronic devices, primarily for optical switching, clock recovery, pulse reshaping, and the generation of a coherent resonance output of pulses. General bifurcation analysis related to excitability in different types of laser is reported in Ref. [29] but here we discuss specifically the mechanism of excitability for a blue InGaN laser of practical design and consider two possibilities to achieve excitable behavior in such lasers.

We begin by considering what is predicted to happen if the carrier lifetime in the SA is increased from 0.1 to 2 ns (the value in the active region) for a laser with a cavity length of 650 μm and a SA thickness of 2 nm. The results of the numerical calculations of photon number against injected current are shown in Fig. 5. For a SA carrier lifetime of 0.1 ns the laser exhibits, as mentioned earlier, self-pulsations as a result of the Hopf bifurcations marked by the squares in Fig. 5(a). With increasing SA carrier lifetime, the pulsation region decreases as shown in Fig. 5(b). The carrier lifetime of 1.4 ns, to which Fig. 5(c) refers, is considered the critical value, after which the hysteresis phenomenon implicit in Fig. 5(d) (corresponding to a lifetime of 2 ns) appears. A further increase of SA carrier lifetime is accompanied by a decrease of the size of the pulsation region and more pronounced hysteresis. A linear stability analysis shows that the lower branch of the hysteresis curve is stable while the upper one is unstable. For the same current, a stable node, a saddle, and an unstable focus are present, providing conditions that can result in excitable behavior. In fact, we have found that when the operating point is situated in the current range denoted by (e) in Fig. 5(d), the laser is excitable. We have also found that the phenomenon of excitability becomes more pronounced as the cavity length is increased. We note that excitability has been predicted to occur when the carrier lifetimes in the active and SA regions are the same, in contrast to the conditions for self-pulsation, where a significantly shorter lifetime in the SA is required. This means that excitability could be achieved in practice in a device where the saturable absorber is made of the same material as the active region and is located next to it in the longitudinal direction.

An alternative approach to obtaining excitability is to have a suitable value for the absorption level. Figure 6 shows

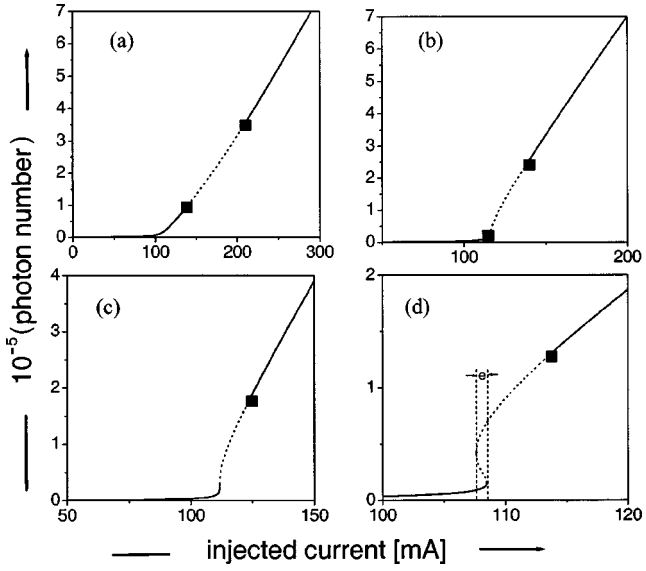

FIG. 5. Dependence of stationary photon number S on the injected current for different values of the carrier lifetime in the saturable absorber. The cavity length is 650 μm and the carrier lifetime is (a) τ_s(SA)=0.1 ns, (b) τ_s(SA)=1.0 ns, (c) τ_s(SA)=1.4 ns, (d) τ_s(SA)=2.0 ns. The thickness of the saturable absorber is 2 nm. The other parameters are as in Table I. The squares represent the Hopf-bifurcation points. In the range "e" the laser shows excitable behavior.

a bifurcation diagram in the plane of SA differential gain coefficient versus injected current for a laser with a cavity length of 650 μm and carrier lifetimes of 2 and 0.5 ns in the active and SA regions, respectively. For $a_{SA}<12\times10^{-12}$ m^3 s^{-1} the laser shows either CW or nonlasing operation for any value of injected current. However, an in-

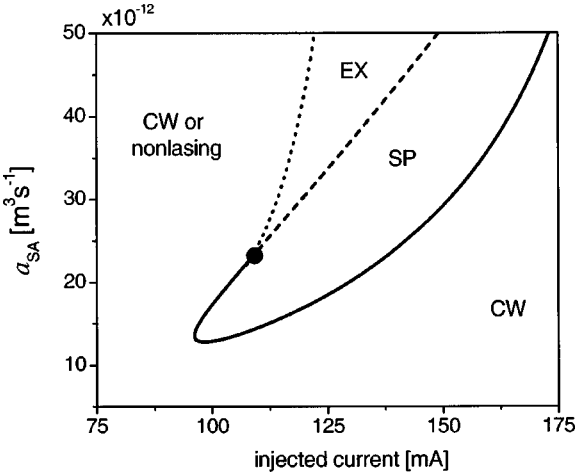

FIG. 6. The bifurcation diagram in the plane of saturable absorber differential gain coefficient vs injected current for a laser with a cavity length of 650 μm and a saturable absorber thickness of 2 nm. The carrier lifetimes in the active region and in the saturable absorber are 2 and 0.5 ns, respectively. The other parameters are as in Table I. The laser behaviour in the different regions is denoted by excitable (EX), self-pulsating (SP), and CW or nonlasing. The solid line represents a Hopf-bifurcation line.

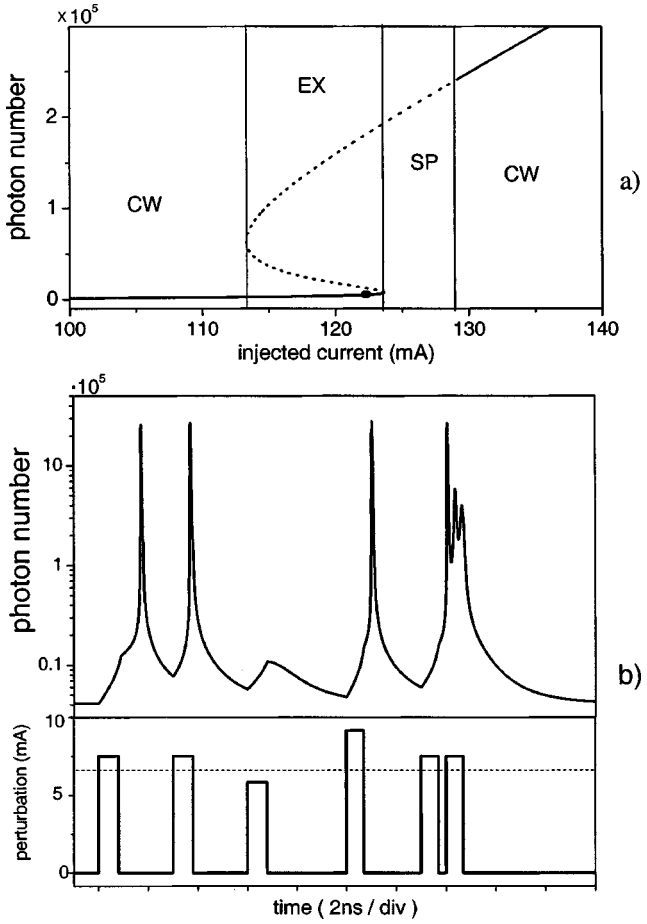

FIG. 7. (a) The different regimes of behavior in the output number injected current plane for a laser with a cavity length of 650 μm, saturable absorber thickness of 2 nm, the saturable absorber differential gain coefficient is fixed to 23×10^{-12} m^3 s^{-1}, carrier lifetimes are 2 ns in both active and saturable absorber regions. (b) Response of the system to a train of pulses with different amplitudes and time separations perturbing the injected current. The initial conditions correspond to the circle in Fig. 7(a). The dotted line denotes the excitability threshold.

crease of the differential gain coefficient of the SA causes the system to cross the Hopf bifurcation indicated by the solid thick line in Fig. 6. Further increase of the differential gain coefficient of the SA results in a homoclinic bifurcation, which is denoted by the filled circle in Fig. 6. Between the dotted and dashed lines, excitability is found to occur. The implication of the figure is that, to achieve excitability in practice by this approach, we need a sufficiently high value of SA differential gain coefficient. However, increasing the SA differential gain coefficient increases both the absorption level and the injected current.

As was mentioned above the existence of excitability is determined by the carrier lifetimes, the absorption level in the saturable absorber and the cavity length. Let us now consider the case of a more pronounced excitability. Figure 7(a) shows the different types of system behavior found in the photon number—injected current plane for large values of carrier lifetime in both the active and the SA regions (2 ns) and high absorption level ($a=23\times10^{-11}$ m^3 s^{-1}) with a 650 μm cavity length. When the injected current is smaller than 114 mA, the laser shows only CW operation, corresponding to the existence of a stable stationary state (stable focus). For injected currents between 114 and 124 mA, a linear stability analysis shows the existence of a saddle close to a stable node, which is well known to provide a mechanism for excitability. A confirmation that excitability is actually predicted in this case is given below. When the injected current is in the range 124–128 mA the laser shows self-pulsation operation, corresponding to the presence of a limit cycle. A further increase of injected current results in CW operation. As a result we are led to conclude that a large carrier lifetime in the SA, a high absorption level and a large cavity length are required to achieve pronounced excitability.

Figure 7(b) shows the response of the laser to a sequence of injected current pulses with different amplitudes and delay times when it is a state within the excitability region [circle in Fig. 7(a)]. There is a substantial response when an input pulse exceeds a certain threshold (such as for the first perturbation pulse) while the response to pulses below the threshold (such as the third pulse) is much smaller. Comparison of the effect of the first and fourth pulses shows that the response is essentially independent of the perturbation amplitude as long as it is above threshold. Further, there is evidence of a refractory period, since when the two pulses are separated by a sufficiently short time interval (such as the fifth and sixth pulses), the later pulse has an insignificant effect on the system. On the other hand, there is clear evidence of a significant response to both pulses when they are separated by a sufficiently large time interval (compare first and second pulses). Taken together the above properties are a clear indication of the presence of excitability in the system. Specifically, we have been able to confirm the three characteristics of excitability: the existence of a threshold above which an excitation can occur; a response independent of the magnitude of a perturbation above threshold; and the existence of a refractory period. Finally, we need to mention that still getting experimental excitable behavior of InGaN lasers is accompanied by difficulties. However, we expect that the phenomena of excitability could be observed in the lasers with cavity length larger than 650 μm and thick AlGaN layer, which results in the larger carrier lifetime in the SA. We believe that our work provides a good basis for future study and, in particular provides some pointers for more detailed investigations of excitability and coherence resonance in InGaN lasers and their possible practical applications.

IV. CONCLUSIONS

We have carried out an investigation of the dynamics of blue-violet InGaN lasers with a saturable absorber. A bifurcation analysis shows that a Hopf bifurcation is responsible for the appearance of self-pulsation under suitable conditions. Also two different possibilities to obtain excitable behavior of the devices have been discussed. It has been shown

that a relatively short carrier lifetime in the SA is required for self-pulsation whereas a large one is more appropriate for excitable behavior. Large cavity length and high saturable absorber differential gain coefficient are also favorable for pronounced excitability. The studies of the dynamics of InGaN lasers are still at an early stage and further theoretical and experiment work is necessary for a proper understanding of the mechanisms involved and a full exploration of the potential application of the phenomena [30].

ACKNOWLEDGMENTS

The authors would like to thank Tomoki Ohno, Shigetoshi Ito, Toshiyuki Kawakami, and Mototaka Taneya from the Devices Technology Research Laboratories, Sharp Corporation, Japan for the experimental support and detailed discussions. V.Z.T. acknowledges the financial support through the Japan Society for the Promotion of Science (JSPS) and from Royal Society/NATO and Alexander von Humboldt Foundation grants.

[1] S. Nakamura, M. Senoh, S. Nagahama, N. Iwasa, T. Yamada, T. Matsushita, Y. Sugimoto, and H. Kiyoku, Appl. Phys. Lett. **69**, 1568 (1996).
[2] For a review, see, S. Nakamura, S. Pearton, and G. Fasol, *The Blue Laser Diode*, 2nd ed. (Springer, Berlin, 2000).
[3] T. Takeuchi, H. Takeuchi, S. Sota, H. Sakai, H. Amano, and I. Akasaki, Jpn. J. Appl. Phys., Part 2 **36**, L177 (1997).
[4] T. Kobaiasi, T. Kobayashi, F. Nakamura, K. Naganuma, T. Tojyo, H. Nakajima, T. Asatsuma, H. Kawai, and M. Ikeda, Electron. Lett. **34**, 1494 (1998).
[5] A. Kuramata, S. Kubota, R. Soejima, K. Domen, K. Horino, and T. Tanahashi, Jpn. J. Appl. Phys., Part 2 **37**, L1373 (1998).
[6] M. Kuramoto, C. Sasaoka, Y. Hisanaga, Y. Hisanaga, A. Kimura, A. A. Yamaguchi, H. Sunakawa, N. Kuroda, M. Nido, A. Usui, and M. Mizuta, Jpn. J. Appl. Phys., Part 2 **38**, L184 (1999).
[7] M. Kneissl, D. P. Bour, C. G. Van de Walle, L. T. Romano, J. E. Northrup, R. M. Wood, M. Teepe, and N. M. Johnson, Appl. Phys. Lett. **75**, 581 (1999).
[8] M. Yamada, J. Appl. Phys. **79**, 61 (1996).
[9] S. Matsui, H. Takiguchi, H. Hayashi, S. Yamamoto, S. Yano, and T. Hijikata, Appl. Phys. Lett. **43**, 219 (1983).
[10] S. Nakamura, M. Senon, S. Nagahama, N. Iwasa, T. Yamada, T. Matsushita, H. Kryoku, Y. Sugimoto, T. Kozaki, H. Umemoto, M. Sano, and K. Chocho, Jpn. J. Appl. Phys., Part 2 **36**, L1568 (1997).
[11] J. D. Murray, *Mathematical Biology* (Springer, Berlin, 1990).
[12] S. Grill, V. S. Zykov, and S. C. Mueller, J. Phys. Chem. **100**, 19082 (1996).
[13] W. Lu, D. Yu, and R. G. Harrison, Phys. Rev. A **58**(2), R809 (1998).
[14] V. Z. Tronciu and R. A. Abram, Phys. Rev. E **65** 026616 (2002).
[15] J. L. A. Dubbeldam, B. Krauskopf, and D. Lenstra, Phys. Rev. E **60**, 6580 (1999).
[16] M. Giudici, C. Green, G. Giacomelli, U. Nespolo, and J. R. Tredicce, Phys. Rev. E **55**, 6414 (1997); **58**, 4043 (1998); G. H.M. Van Tartwijk and I. Fischer, *ibid.* **58**, 4041 (1998); E. A. Viktorov and P. Mandel, Phys. Rev. Lett. **85** 3157 (2000); J. R. Tredicce in *Nonlinear Laser Dynamics: Concepts, Mathematics, Physics, and Applications*, edited by Bernd Kranskopfand Daan Lenstra, AIP Conf. Proc. No. 548 (AIP, Melville, NY, 2000), p. 238.
[17] V. Z. Tronciu, H. J. Wünsche, K. Schneider, and M. Radziunas, Proc. SPIE **4283**, 347 (2001).
[18] H. J. Wünsche, O. Brox, M. Radziunas, and F. Henneberger, Phys. Rev. Lett. **88**, 023901 (2002).
[19] M. A. Larotonda, A. Hnilo, J. M. Mendez, and A. M Yacomotti, Phys. Rev. A **65**, 033812 (2002).
[20] M. Yamada, IEEE J. Quantum Electron. **29**, 1330 (1993).
[21] M. Yamada, IEICE Trans. Electron. **E81–C**, 290 (1998).
[22] L. A. Dubbeldam and B. Krauskopf, Opt. Commun. **159**, 325 (1999).
[23] C. R. Mirasso, G. H. M. van Tartwijk, E. Hernandez-Garcia, S. Lynch, P. Landais, P. Phelan, J. O'Gorman, M. San Miguel, and W. Elsasser, IEEE J. Quantum Electron. **35**, 764 (1999).
[24] T. Ohno, S. Ito, T. Kawakami, and M. Taneya, Appl. Phys. Lett. **83**, 1098 (2003).
[25] M. Yamada, IEEE J. Quantum Electron. **30**, 1511 (1994).
[26] Shigetoshi Ito, Yukio Yamasaki, Susumu Omi, Kunihiro Takatani, Toshiyuki Kawakami, Tomoki Ohno, Masaya Ishida, Yoshihiro Ueta, Takayuki Yuasa, and Mototaka Taneya (unpublished).
[27] Y. D. Jho, J. S. Yahng, E. Oh, and D. S. Kim, Appl. Phys. Lett. **79**, 1130 (2001).
[28] C.-K. Sun and T.-L. Chiu, Appl. Phys. Lett. **71**, 425 (1997).
[29] B. Krauskopf, K. Schneider, J. Sieber, S. Wieczorek, and M. Wolfrum, Opt. Commun. **215**, 367 (2003).
[30] T. Yuasa, Y. Ueta, Y. Tsuda, A. Ogawa, M. Taneya, and K. Takao, Jpn. J. Appl. Phys., Part 2 **38**, L703 (1999).